Theoretical and Applied Mechanics 2000

Volume I

Editor
G. G. Sih

Tsinghua University Press

MESOMECHANICS 2000

Role of Mechanics for Development of Science and Technology

Volume I

Role of Mechanics for Development of Science and Technology

Proceedings of an International Conference of Role of Mechanics for Development of Science and Technology, held at Xi'an Jiaotong University, Xi'an, China, June 13-16, 2000

Edited by

G.C. Sih

Department of Mechanical Engineering and Mechanics,
Lehigh University, Bethlehem, Pennsylvania, USA

Volume I

Tsinghua University Press
Beijing, China

MESOMECHANICS 2000

Proceedings of the Third International Conference for Mesomechanics

Xi'an, P.R. China

Editor: G.C. Sih

Tsinghua University Press

Beijing 100084, P.R. China

Tsinghua

ISBN 7-302-00979-1/O • 231 Set of 2 Volumes

Numerical simulation of deformation and fracture for surface hardened materials at meso- and macro- levels.

R.R. Balokhonov, Yu.P. Stefanov, P.V. Makarov, I.Yu. Smolin

Institute of Strength Physics and Materials Science, Russian Academy of Sciences, Siberian Branch, 634021, Tomsk, Russia.

Abstract

Investigated in this work is the plastic deformation of representative mesovolumes of the steel 65Cr13 sample. It was surface hardened by ion nitriding. An evolution of inner structure and stress-strain state in the mesovolumes with different thickness of surface hardened layer were analyzed under tension and compression. A site of the working part of a cross section of the sample was examined in the area of neck formation. To simulate the two-dimensional behavior of the deformed steel sample, two formulations are given. They include the strain hardening effects and crack formation. The results are presented and discussed.

1. Introduction

Majority of the structural components and machine parts used in industry have coatings or are surface hardened. Therefore, experimental and theoretical research of coated materials under load are important and could provide useful information to engineering application.

According to physical mesomechanics, a solid under loading is a highly nonequilibrium self-organizing system where the deformation and fracture process occur at the micro-, meso- and macrolevel [1,2]. To study the plastic deformation process, it is essential to identify the key scale level that controls the behavior of plastic flow for a given loading. The development of the mesoscopic mechanisms of plastic deformation makes itself even more evident in coated and surface-hardened materials in addition to those experiencing fatigue fracture. The resulting material substructure is determined by the level of the mesoscopic stress concentrators involved and dependent on the relation between mechanical properties of the coating and substrate including their thickness ratio.

Earlier, the physical mesomechanics approach was applied successfully to numerical simulation of the process of ultrasonic surface treatment [3] and the process of localized deformation in mesovolumes of polycrystalline materials [4].

The main aim of this work is to investigate numerically the behavior of coated steel specimens under tension and compression. The mesoscopic deformation process were simulated by a two-dimensional formulation in plane-strain. Numerical solutions were performed in terms of Lagrangian variables using finite-difference of the second order of accuracy [5]. Calculations pertain to plastic flow at the meso- and macroscale levels. At the mesolevel, the mesovolumes of the material were considered being deformed up to the formation of the bands of localized plastic deformation when the coating gets distorted.

Another set of calculations are made to simulate the behavior of a macrofragment of a flat coated specimen in tension. A special feature of this approach is an explicit account of the crack nucleation and growth when examining the interplay between plastic strains in the substrate and cracks in the coating that would affect the overall stress-strain state of the system.

2. Mathematical definition

The system of equations for plane flow of the medium is adopted. Fo plane-strain, the displacement field is

$$\mathbf{u} = \{u_1, u_2, 0\} \tag{1}$$

The corresponding non-zero components of strain rate are given by

$$\dot{\varepsilon}_{11} = \dot{u}_{1,1}, \quad \dot{\varepsilon}_{22} = \dot{u}_{2,2}, \quad \dot{\varepsilon}_{12} = \frac{1}{2}\left(\dot{u}_{1,2} + \dot{u}_{2,1}\right) \tag{2}$$

where u_1 and u_2 are the components of the displacement vector. Dot represents time derivative and comma denotes space derivative. Conservation law takes the form

$$\dot{\rho} + \rho \cdot (\dot{u}_{1,1} + \dot{u}_{2,2}) = 0 \tag{3}$$

where ρ is the mass density. The equations of motion are

$$\sigma_{11,1} + \sigma_{21,2} = \rho\ddot{u}_1, \quad \sigma_{12,1} + \sigma_{22,2} = \rho\ddot{u}_2 \tag{4}$$

Here σ_{ij} are stress tensor components. The law of energy balance in the absence of thermal changes and internal heat production takes the form

$$\rho\dot{E} = \sigma_{11}\dot{\varepsilon}_{11} + \sigma_{12}\dot{\varepsilon}_{12} + \sigma_{21}\dot{\varepsilon}_{21} + \sigma_{22}\dot{\varepsilon}_{22} \tag{5}$$

Note that in the present model at rather low pressure (up to 10 MPa) the linear barotropic equation of state [6] can be used. In this case, it is not necessary to calculate an internal energy. To complete the system of eqs. (1) to (4) a constitutive equation is required. Taking into account the resolution of stress tensor into dilatational and deviatoric parts

$$\sigma_{ij} = -P\delta_{ij} + S_{ij} \tag{6}$$

Incompressibility required that $\dot{\varepsilon}^p_{kk} = 0$. Non-zero components of force stress tensor are given by

$$\dot{S}_{11} = 2\mu\left(\dot{\varepsilon}^e_{11} - \frac{1}{3}\dot{\varepsilon}^e_{kk}\right), \qquad \dot{S}_{22} = 2\mu\left(\dot{\varepsilon}^e_{22} - \frac{1}{3}\dot{\varepsilon}^e_{kk}\right),$$

$$\dot{S}_{12} = 2\mu\dot{\varepsilon}^e_{12}, \qquad \dot{S}_{33} = 2\mu\left(-\frac{1}{3}\dot{\varepsilon}_{kk}\right) = -\left(\dot{S}_{11} + \dot{S}_{22}\right) \tag{7}$$

Note that

$$\dot{P} = -K\dot{\varepsilon}_{kk} \tag{8}$$

Here, K is the bulk modulus and μ is the shear modulus while δ_{ij} is the Kronecker delta.

2.1 Plastic flow strain hardening

To elucidate the peculiarities of deformation at the mesolevel, strain hardening for individual grains will be incorporated in the constitutive equations. In this case the yield criterion is of the form

$$\sigma_{eff} - f\left(\int d\varepsilon_{eff}\right) = 0 \tag{9}$$

where f is a function that specifies hardening of grains of the mesovolume under study, i.e.,

$$\sigma_{eff} = \frac{1}{\sqrt{2}}\left\{(S_{11} - S_{22})^2 + (S_{22} - S_{33})^2 + (S_{33} - S_{11})^2 + 6\left(S^2_{12} + S^2_{23} + S^2_{31}\right)\right\}^{\frac{1}{2}} \tag{10}$$

and

$$\varepsilon^p_{eff} = \frac{\sqrt{2}}{3}\left\{\left(\varepsilon^p_{11} - \varepsilon^p_{22}\right)^2 + \left(\varepsilon^p_{22} - \varepsilon^p_{33}\right)^2 + \left(\varepsilon^p_{33} - \varepsilon^p_{11}\right)^2 + 6\left(\varepsilon^{p\,2}_{12} + \varepsilon^{p\,2}_{23} + \varepsilon^{p\,2}_{31}\right)\right\}^{\frac{1}{2}} \tag{11}$$

Substituting

$$\dot{\varepsilon}^e_{ij} = \dot{\varepsilon}_{ij} - \dot{\varepsilon}^p_{ij} \tag{12}$$

into eqs. (7) and considering the associated flow rule with the criterion given by eq. (9) for the plastic part of strain rate tensor

$$\dot{\varepsilon}^p_{ij} = \dot{\lambda}S_{ij} \tag{13}$$

the constitutive equations for the stress deviators are obtained:

$$\dot{S}_{11} = 2\mu\left(\dot{\varepsilon}_{11} - \frac{1}{3}\dot{\varepsilon}_{kk}\right) - 2\mu\dot{\lambda}S_{11}, \qquad \dot{S}_{22} = 2\mu\left(\dot{\varepsilon}_{22} - \frac{1}{3}\dot{\varepsilon}_{kk}\right) - 2\mu\dot{\lambda}S_{22};$$

$$\dot{S}_{33} = 2\mu\left(-\frac{1}{3}\dot{\varepsilon}_{kk}\right) - 2\mu\dot{\lambda}S_{33} = -\left(\dot{S}_{11} + \dot{S}_{22}\right), \qquad \dot{S}_{12} = 2\mu\dot{\varepsilon}_{12} - 2\mu\dot{\lambda}S_{12} \tag{14}$$

Here, λ is a scalar plastic flow rate parameter which is defined from the following equation

$$\lambda = \frac{3A^{pl}}{2f\left(\int d\varepsilon_{eff}\right)} \tag{15}$$

where A^{pl} is the plastic energy rate.

2.2 Crack formation

Fracture of material is simulated on the basis of an algorithm for splitting the grid nodes. Cracks grow along the borders of the cells. This rules out the problems connected with the fulfilment of the conservation laws in the zone of fracture. The newly formed surfaces are considered to be stress free. When describing fracture, use was made of the stress fracture criterion of the form

$$\alpha\sigma_n + (1-\alpha)\sigma_\tau = \sigma_o \tag{16}$$

Here, σ_n is the normal stress and σ_τ is the tangential stress that is calculated at the borders of the cells as averaged over two adjacent cells. The critical stress is σ_o.

2.3 Initial and boundary conditions

Consider a domain $D(\boldsymbol{x},t)$ with the boundary $\Gamma(\boldsymbol{x},t)$, where x is the radius vector and t is the time. Initial conditions at $t = 0$ for every $\boldsymbol{x} \in D(\boldsymbol{x},0)$ have the form:

$$\dot{u}_i(x) = v_i^{(o)}(x), \quad \sigma_{ij}(x) = \sigma_{ij}^{(o)}(x) \qquad \text{for } i, j = 1, 2 \tag{17}$$

Assume that

$$\rho(x) = \rho^{(o)}(x)$$

For mixed boundary conditions, there prevails

$$\dot{u}_i(\boldsymbol{x},t) = v_i^{(\Gamma)}(\boldsymbol{x},t) \qquad \text{for } t \geq 0 \text{ and } \boldsymbol{x} \in \Gamma_1; \tag{18}$$

while

$$\sigma_{ji}(\boldsymbol{x},t) \cdot n_j = p_i^{(\Gamma)}(\boldsymbol{x},t) \qquad \text{for } t \geq 0 \text{ and } \boldsymbol{x} \in \Gamma_2 \tag{19}$$

where i, j = 1, 2 and

$$\Gamma = \Gamma_1 \cup \Gamma_2 \tag{20}$$

The vector components normal to the surface are n_j.

3. Results of numerical simulation

Fig. 1 shows a map of the test section. The original internal inhomogeneity of the medium was given explicitly in the calculation. Each of the elements of the internal structure was

assigned unique mechanical characteristics. The simulations reproduced a real structure and actual dimensions of a representative mesovolume. The area under study comprised an estimated 500 grains with an average size range of about 20 to 30 μm, Fig. 1. The calculations assumed coating thicknesses of 25 and 80 μm. The spread in mechanical characteristics of different grains was prescribed arbitrarily. An individual grain was assigned a particular function f corresponding to a specific curve for the range δ of the hardening function, Fig. 2. This accounts for the spread of the mechanical characteristics about their mean values caused by different orientations of individual grains in the substrate. In regions A and B (Fig. 1) average characteristics representative of the properties of an untreated specimen were introduced, as shown in Fig. 2. For specimens with coating, higher strength properties were assigned. The hardening function for the coating was taken to be a constant f = 1100 MPa. In the calculations, the boundary conditions in eqs. (17) and (18) for uniaxial loading (Fig. 1) are given as

$$\begin{aligned} &\text{BC1: } u_x = -v = \text{const}, \quad \text{BC3: } u_x = v, \\ &\text{BC2: } \sigma_{ij} n_j = 0, \qquad\quad \text{BC4: } u_y = 0 \end{aligned} \tag{21}$$

Boundary conditions at the boundaries BC1 and BC3 simulate the constant clamp displacement, while at the boundaries BC2 and BC4 they correspond to the free surface condition and symmetry condition, respectively.

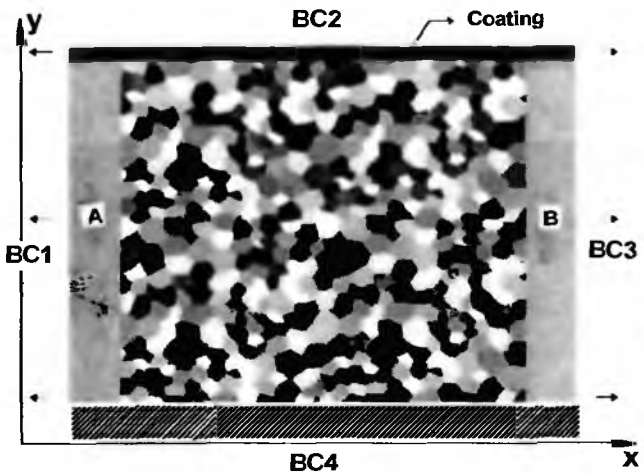

Fig. 1 Original structure of mesovolume

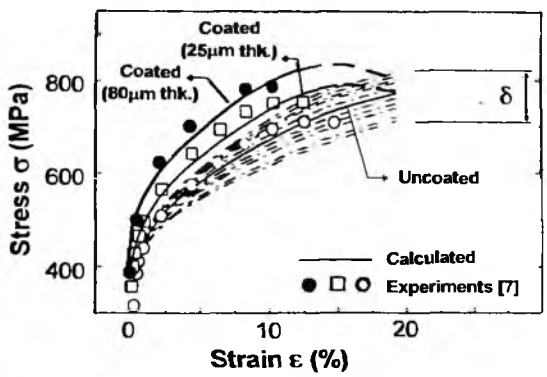

Fig. 2 Stress-strain curves for 65Cr13 steel

Fig. 3(a) and 4(a) show a Lagrangian coordinate grid with isolines of the plastic strain intensity (or effective strain). For comparison purposes, Figs. 3(b) and 4(b) give optical images of lateral faces of specimens with different thickness of coating. The calculations show that plastic deformation in the prefracture stage becomes localized in the direction closely matching at of maximum tangential stress. The subsurface layer exhibits "corrugation" whose amplitude and wavelength depend on the thickness of the coating and the degree of internal inhomogeneity of the substrate. As the coating becomes the larger blocks tend to separate by localized plastic deformation bands, they are formed in the base material but

cannot be seen in Figs. 3(a) and 4(a). The "corrugation" parameters obtained in the simulations agree fairly well with the experimental evidence obtained in [7]. Refer to Figs. 3(b) and 4(b). Additional loading and the influence of a macroscopic stress concentrator near the surface cause deformation to become localized along a most favorable direction and a neck is subsequently formed that is shown in Fig. 5(a). This stage of plastic deformation corresponds to the descending portion of the stress-strain curve, Fig. 2. Displayed are the integral experimental and calculated stress-strain curves for specimens with different coating thicknesses as specified on the curves. The stress was calculated as an average stress intensity over all cells of the computational grid. The strain was determined as a percentage of extension of the tested mesovolume. Note that good quantitative agreement is obtained for the results of the calculation and experiment.

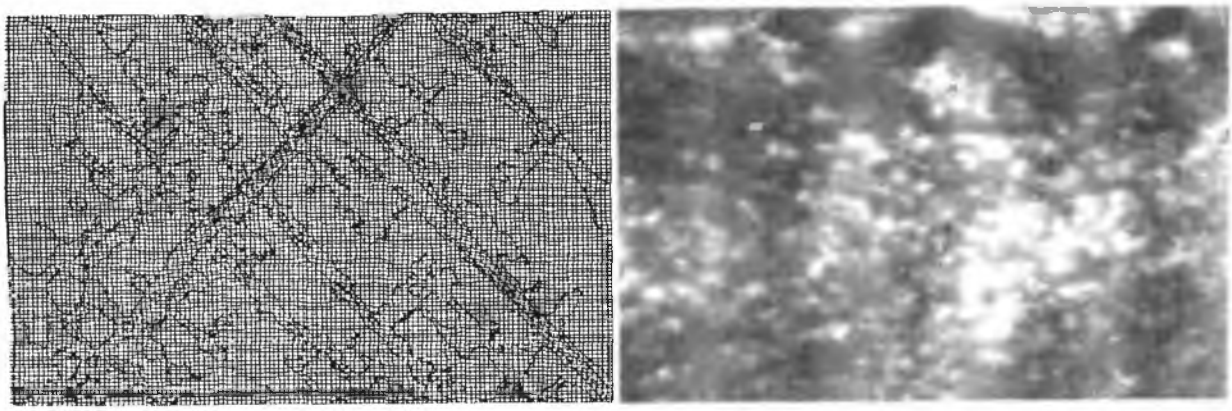

(a) Calculation (b) Experiment [7]

Fig. 3 Distribution of shear bands for tensile strain of 12% and coating thickness of 30 μm

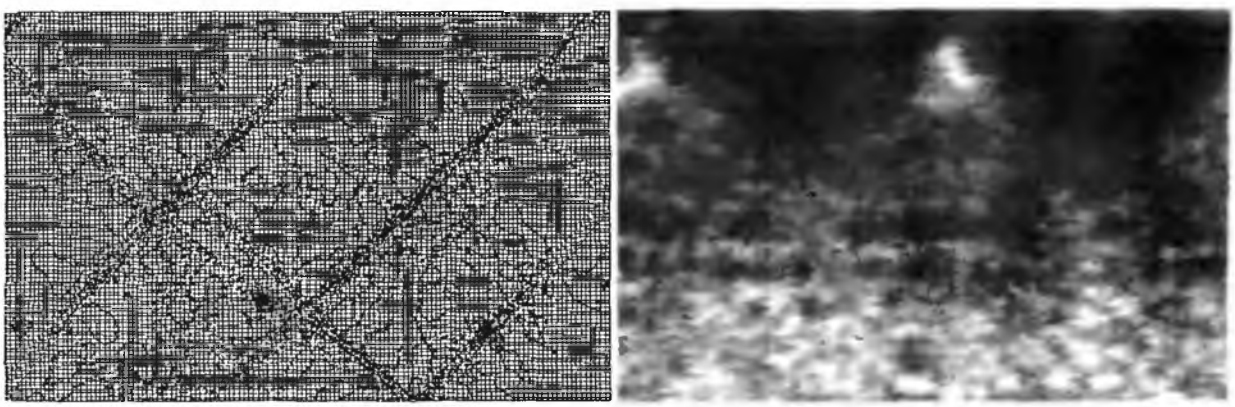

(a) Calculation (b) Experiment [7]

Fig. 4 Distribution of shear bands for tensile strain of 12% and coating thickness of 80 μm

Calculations for compression of mesovolume were carried out for equal coating thickness. The type of loading influences the type of formed mesodefective structure only slightly as shown in Fig. 3(a) and 5(b). The character of localized plastic deformation (Fig. 5) is slightly influnced. In both cases (tension and compression), the fragmented structure with certain

characteristic size is formed. However, under tension, one shear band is precisely formed in a certain direction that corresponds to neck formation, Fig. 5(a). Under compression this direction is not the most favorable, Fig. 5(b). The deformation is located in several directions. Neck is not formed, and separate blocks are squeezed to a surface.

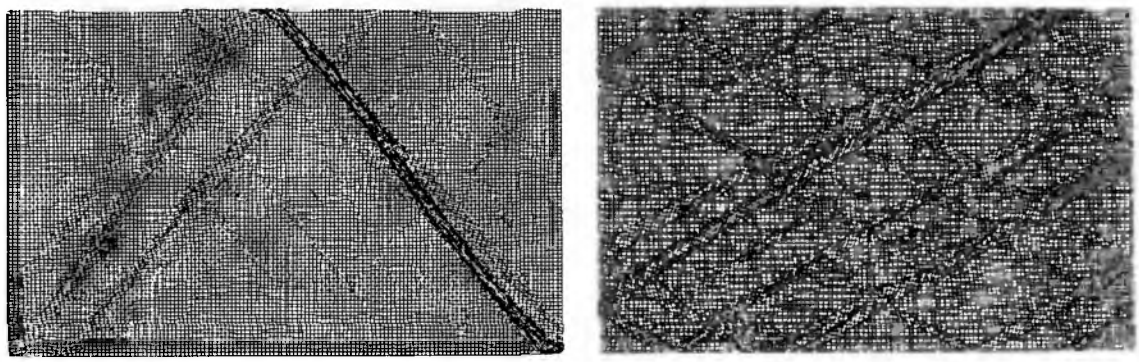

(a) Tension (b) Compression

Fig. 5 Distribution of shear bands for tensile strain of 15% and coating thickness of 30 μm

The stress-strain state is calculated for structural steel specimen subjected to surface-hardening on both sides (~150 μm layer thickness). A numerical model is applied to estimate crack nucleation and growth. The model assumes that a test material will fail when tensile stresses reach their critical values. A schematic sketch of a test specimen with numerical values of geometric characteristics of the computational area is presented in Fig. 6. The hardened layers are assumed to be elastic. The base material is assumed to be elastic-perfectly plastic. To avoid direct influence of the "hard" clamps to cracking, the fracture criterion was not checked in the regions close to the clamps. The hardened layers bear the major load up to the point of cracking. As single cracks are formed, the hardened layers become unloaded, stresses increase, and deformation at the crack tips intensities. Originating from the crack tip along the direction of maximum tangential stress, there prevails the localized plastic deformation bands whose occurrence at the opposite sides of the specimen may cause its surface layers to crack. From this point on, the behavior of the specimen will depend on the relation between the strength properties of the hardened layers and ductility of the substrate. If the stress level in the substrate is sufficiently high to initiate new cracks in the hardened layers, further formation of localized shear bands will occur and the hardened layers will crack along the entire surface of the specimen (Fig. 7). At low stresses, the specimen cross section will tend to reduce and either a neck will develop or the main crack will grow. Even with a perfectly homogeneous substrate, a slight difference between the properties or thicknesses of the top and bottom hardened layers will result in non-uniform (skewed) stress and strain distributions. Since the cracks across the two flat faces (top and bottom layers) of the specimen in an asymmetric manner and occur at different instants of time, this effect tends to enhance the specimen distortion. In Fig. 8(a), localized shear bands oriented along the directions of maximum tangential stress are seen to join the cracks at the hardened layers in the opposite sides of the specimen. A similar deformation pattern was observed experimentally in Figs. 8(b) and 8(c) as in [9].

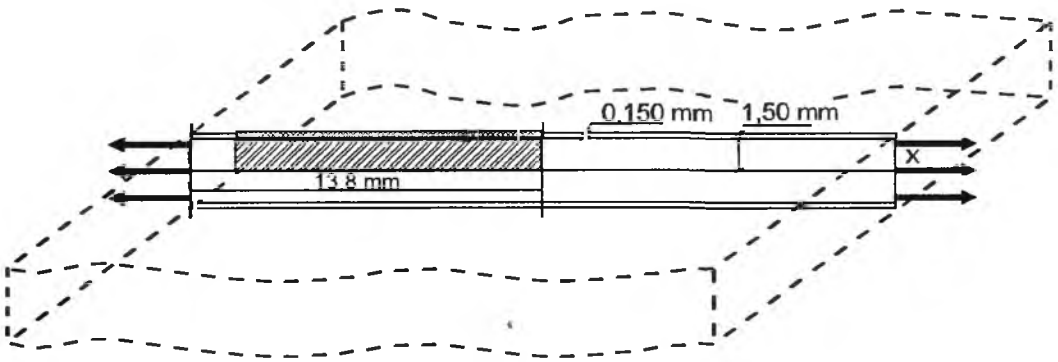

Fig. 6 A schematic view of calculation region (hatched)

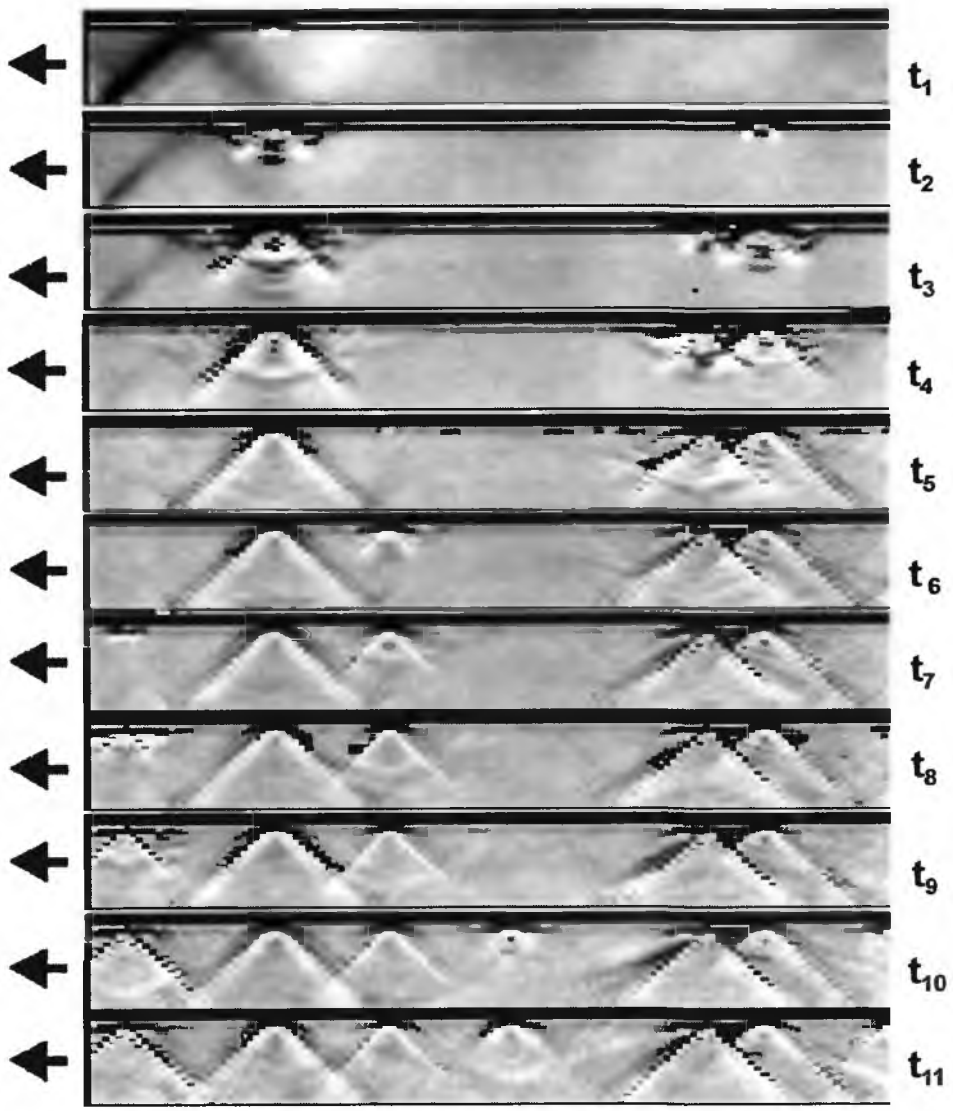

Fig. 7 Plastic strains for cracks in hardened layer under tension

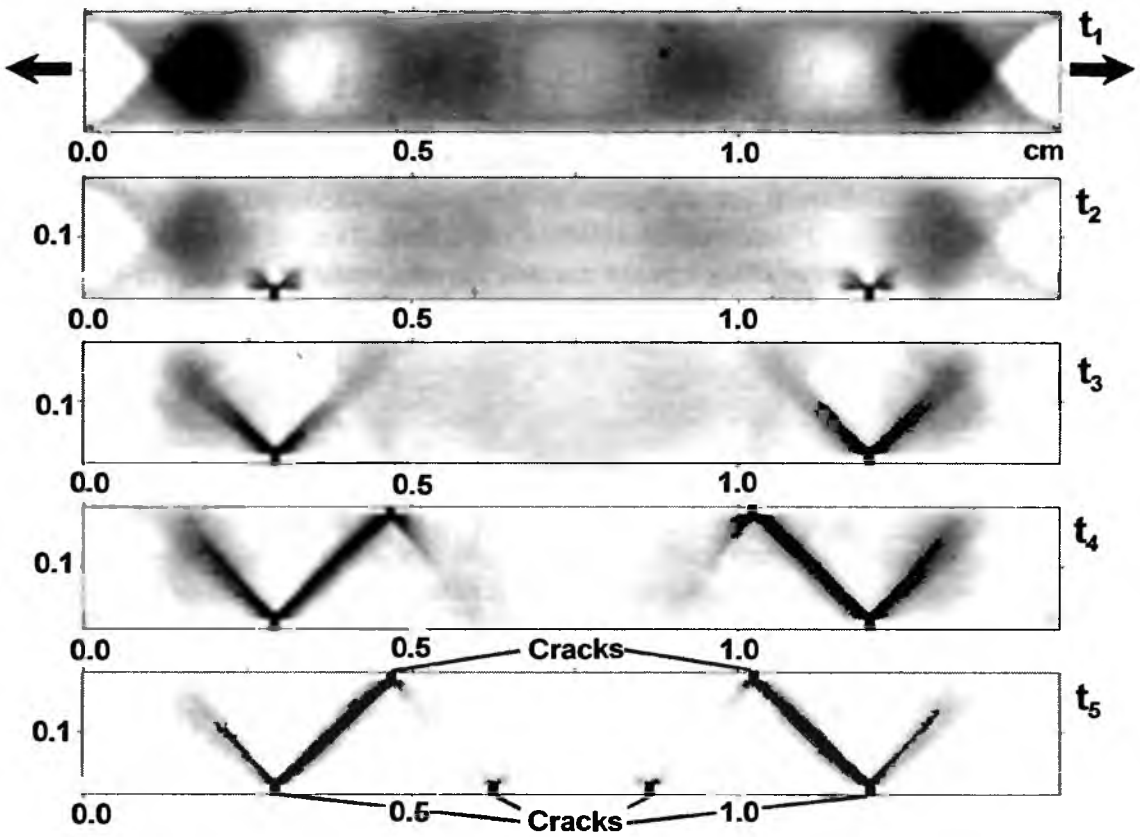

(a) Plastic deformation distribution

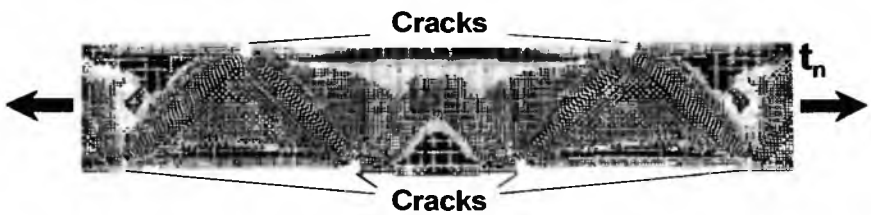

(b) Bending in calculations

(c) Bending in experiment [7]

Fig. 8 Development of the localized deformation bands during cracking of hardened layer in tension of surface hardened sample (a) and bending of the sample (b), (c)

4. Conclusion

The computer simulation of deformation in the mesoscopic volumes of coated materials show that the coating thickness is an important factor. It governs the localization pattern of plastic deformation in the prefracture stage in regions where the mechanical characteristics of the coating and the substrate are different in the surface-hardened material subjected to tension and compression. Numerical simulation of deformation in material with hardened layers suggest that transverse cracks in the surface layers (being strong stress concentrators) play a decisive role in straining and fracture of specimens with thick hardened layers.

Acknowledgment

Support from the Russian Foundation for Basic Research through the project 99–01–00583 is gratefully acknowledged.

References

[1] *Physical Mesomechanics of Heterogeneous Media and Computer-Aided Design of Materials*, in: V.E. Panin (ed.), (Cambridge International Science Publishing, Cambridge, 1998).

[2] V.E. Panin, A.D. Korotaev, P.V. Makarov, V.M. Kuznetsov, Physical mesomechanics of materials, *Russian Physics Journal,* 9, 8-36 (1998).

[3] P.V. Makarov, V.A. Romanova, R.R. Balokhonov, Plastic deformation behavior of mild steel subjected to ultrasonic treatment, *Theoretical and Applied Fracture Mechanics,* 28, 141-146 (1997).

[4] P.V. Makarov, I.Y. Smolin, I.P. Prokopinsky, Localized plastic strain in polycrystalline materials with hole and notches, *Theoretical and Applied Fracture Mechanics,* 29, 11-20 (1998).

[5] M.L. Wilkins, Calculations of elastic-plastic flow, in: B. Alder, S. Fernbach, M. Rotenberg (eds.). *Methods in Computational Physics*, Vol. 3, (Academic Press, New York, 211-263, 1964).

[6] D. Kolarov, A. Baltov, N. Boncheva, *Mechanics of Plastic Media*, (Mir Publishers, Moscow, 1979).

[7] V.E. Panin, A.I. Slosman, N.A. Kolesova, Laws of plastic deformation and fractures at the mesolevel of surface hardened samples under static tension, *Fizika Metallov i Metalovedenie,* 82, 129-136 (1996).